SEMARAK ILMU PUBLISHING

Journal of Advanced Research in Applied Mechanics

Journal homepage:
https://semarakilmu.com.my/journals/index.php/appl_mech/index
ISSN: 2289-7895

Evaluation of Modified Ductile Ni-Resist Alloy Solidification with Higher Chromium and Manganese

Muhammad Aminuddin Rosnizan[1], Mohamed Reza Zalani[1], Khairul Ihsan Yaakob[1], Fatin Syairah[1], Mohd Rashidi Maarof[1,2,*]

[1] Manufacturing Research Focus Group (MFG), Faculty of Mechanical and Automotive Engineering Technology, Universiti Malaysia Pahang (UMP), 26600 Pekan, Pahang, Malaysia
[2] Automotive Engineering Centre, Universiti Malaysia Pahang (UMP), 26600 Pekan, Pahang, Malaysia

ARTICLE INFO

Article history:
Received 24 October 2024
Received in revised form 25 November 2024
Accepted 2 December 2024
Available online 30 December 2024

Keywords:
Metal casting; solidification; Ni-Resist; nodularisation; inoculation; segregation

ABSTRACT

These days, batteries, applications requiring high temperatures, and corrosive environments are the main uses for nickel. The rise in electric and hybrid vehicles has increased the amount of nickel used as the primary component in alloys. Due to manufacturer interest, the price of nickel had reached its apex and was becoming erratic. One compound that is impacted is the Ni-Resist alloy. In this work, the nickel weight % of an alloy known as ductile Ni-resist alloy was reduced in order to reduce processing costs due to nickel price. This effort involved the modification of ductile Ni-resist alloy with a minimum 18 weight percent nickel content with up to 10 weight percent of chromium and manganese which were added during melting stage. The adjustment was looked into in an effort to lessen the cost of the alloying process by using less nickel in the alloying mixture. After that, the microstructure, solidification behavior, and property evaluation were looked at. The findings demonstrate that increased manganese and chromium content on modified ductile Ni-resist alloy affects base iron's DAS and SDAS as well as graphite production. The dimension of DAS and SDAS was minimally altered by the addition of chromium and manganese weight percentage. Following solidification, a distinct kind of DAS and SDAS was seen on the modified ductile Ni-resist.

1. Introduction

Over the past few decades, manufacturers have developed commercial vehicles at a faster pace in an effort to make their products more competitive. In order to stay competitive, extensive research was conducted on new alloy types to guarantee their sustainability or to investigate superior alloys to guarantee the component can be persistent in harsh and demanding environments. The current research has pushed certain alloys to further exploration, including Ni-Resist alloy, which is utilized for dynamic load at elevated temperatures. The alloy known as Ductile Ni-Resist (DNR) is one of the affected subcategories. The Ni-Resist alloy has an austenite structure with nodular graphite

* *Corresponding author.*
E-mail address: mrashidi@umpsa.edu.my

https://doi.org/10.37934/aram.130.1.2737

shapes. Due to its austenitic matrix alloy, which is usable at practically all temperatures, high strength-to-weight ratio, good machinability, and reasonably acceptable mechanical properties at elevated temperatures, Ni-Resist alloy is suitable for high temperature applications. In contrast, applications of cast iron and steel above 675°C temperature traverse a critical area that often results in the possibility of casting deformation and cracking. The deformation occurred due to matrix phase transitions from Body Centered Cubic BCC crystal structure (ferrite) to Face Centered Cubic FCC (austenite), which volume changes were thought to be the cause. Because of their austenitic matrix at all temperatures, DNR alloys lack this transition, making them highly advantageous for applications requiring increased temperatures.

The effective alloying techniques used during melting allow for this transition. The 'nose' of the T-T-T curve is sliding to the right as the alloy solidifies [1]. Therefore, it's possible that the solidification curve will skip the curve and promote the development of an austenitic structure. If the stage is successful, the austenite might stabilize and hold themselves from room temperature until it reaches elevated temperature (more than 675°C). The austenite occurrences were attained without additional heat treatment, thus reducing the total cost of metal casting processes. Compared to costlier austenitic steel, this processing option gives DNR alloy a competitive position in oil and gas, automotive, or power plant components [2].

According to a recent study, nickel (Ni) is successfully utilized as the main alloying element in the production of nickel resists. It happens because nickel's as-cast austenite microstructure is resistant to occurs in the process as a result of the metal composition's action on Ni, which serves as an austenite matrix stabilizer. At a minimum of 18 weight percent, Ni suppresses the austenite (γ) → ferrite (α) transformation into ordinary ductile iron [3]. Nonetheless, Ni is a recognized to be a somewhat costly raw element, and alloying Ni-Resist alloy is economically constrained by its high cost. So, many studies were conducted to lower the Ni/wt% in an effort to curtail production costs. Thirteen weight percent was the least amount of Ni/wt% that was effectively employed to convert alloyed iron to austenite structure. The potential of manganese (Mn) and copper as substitutes for the alloying ingredient nickel resists has been documented in another study [4]. The outcome of the experiment, however, indicated a detrimental impact. Morrison [3] suggests that although copper can create an austenite structure, the process has a negative influence on Nickel resists' nodule graphite.

Mn as another alloying candidate stabilizes the austenite phase but come at a price. Mn encourages the development of carbides. By adding more Mn, free graphite is kept from congealing into nodular graphite. Rather, it promotes the formation of carbide. Additionally, Morrison stated that alloying with less than 4 weight percent Mn is comparable to free carbide nickel resists. To reduce the production of carbide, an inoculation procedure is used as a remedy. According to reports, inoculation can significantly enhance the distribution and graphite shape of traditional ductile iron, as suggested by Jincheng [5]. Furthermore, Choi *et al.,* [6] report that inoculation enhances the undercooling effect during the casting solidification of conventional cast iron. Similarly, he proposed that for typical ductile iron, inoculation can generally enhance the graphite shape and dispersion. So, inoculation technique is suggested as a possible remedy in their inquiry to enhance the undercooling effect during casting solidification.

Solidification cooling curve may be influenced by material structure refinement, according to Jiyang [7]. Rearranging the distribution of the graphite structure rather than the carbide distribution during the inoculation step may accomplish the alteration. This method was used to compare the solidification cooling curves with respect to the undercooling stage. Consequently, there is less of an element segregation and secondary phases, such the region slowest to solidify.

Another study conducted to discover Ni alternative was done for example; Fe-Mn-Al-Si alloy's composition and scale morphology were examined by Anderson and Vanessa [8]. In their research, oxidation resistance has been found to arise between 600 and 900 ^{o}C. Second phases (oxides of Al, Mn, and Fe) followed the oxidation stages and functioned to prevent further oxidation from getting worse. Tjong [9] investigated the potential of producing FeAlMnC by substituting Mn for Cr and Ni. He noticed mechanical qualities that are feasible at cryogenic temperatures in his investigation. Rashidi and Hasbullah [10] adjusted Ni-Resist alloy in the interim and assessed its characteristics and microstructure. The oxidation test was not performed, though. Heat-resistant Si-Mo ductile cast iron's mechanical characteristics and oxidation resistance were examined by Kim *et al.,* [11]. The outcomes demonstrated that alloy enhancement is possible by adjusting individual alloy elements.

The goal of this study is to create an alloy as similar as Ni-Resist alloy by combining Ni, Mn, and Cr at a specific composition. Mn/wt% and Cr/wt% are raised to as high as 10%, while Ni/wt% is decreased to as low as 18%. This composition will be treated by nodularisation and inoculation technique to enhance alloy requirement. In terms of microstructure, the amended alloy should take the form of an austenite structure with a graphite nodule (if magnesium, Mg, is added) or a flake graphite structure (if Mg is not added). The purpose of the study is to investigate how alloying components affect the solidification of alloyed iron. Second, a crucial factor to take into account is the impact of magnesium treatment on the formation of graphite following solidification. The microstructural variability of the casting is given particular attention. The use of DNR alloy exposes components to a somewhat high temperature, which is why the emphasis is considered significant.

2. Methodology

The current investigation was carried out in an induction furnace with a 3 kg holding capacity, 20 kW of power, and a 1000–3000 Hz frequency range. Steel scrap, pig iron, and pure nickel were the charge materials used to create modified alloyed iron with the desired composition, which was 5Mn-5Cr-18Ni. Ferro-Manganese (FeMn) and Ferro-Chrome (FeCr) were added after stirring sessions to raise the amount of manganese and chromium, as shown by Rashidi and Hasbullah [10]. As directed by them, the melt was first superheated to 1500+20^{o}C and cleaned by slag catcher before being placed into a mold at 1400+20^{o}C approximately. Utilizing a mixture of silica sand, bentonite, and water, a green sand mold was produced. Next, magnesium treatment and inoculation were done using the In-mould method. As indicated in Figure 1, 0.5 weight percent inoculation and 1.1 weight percent nodularizer were added to the mold reaction chamber. The chemical compositions of each element, nodularizer, inoculant, nickel, FeMn, and FeCr are listed in Table 1. In order to enhance the dissolve process and lessen the effect of fading, an inoculant with a grading size of 0.2 to 0.7 mm was employed. Following solidification, Y-blocks with the ASTM A439 shape were divided into sections and anchored. A microstructural specimen was obtained by polishing the specimen with 0.3 µm alumina powder later on. Multiple specimens were created with dimensions of 15.0 x 15.0 x 2.0 mm. They were polished with 1.0 µm diamond paste after being mechanically ground to 2400 mesh using SiC paper. After polishing the samples to a mirror sheen, they were gradually cleaned in ethanol and acetone using ultrasonic agitation for ten minutes. The samples were dried and desiccated prior to exposure. The pulverized alloy was analysed using powder XRD to ascertain the phase composition [10]. X-ray energy dispersive spectroscopy (EDS) was used to examine the chemical composition of the scales that had developed on the specimens' surface after they were discovered using a scanning electron microscope (SEM). To protect the scales on a specimen, copper was applied while a cross-sectional metallographic view was being generated. The chemical analysis was performed using the Philips XL40 EDS model system. Phase analysis was performed with a Siemens D5000 X-ray

diffractometer (XRD) utilizing CuK-1 radiation. 2 sample was compared, the 1st without reaction with MgFeSi and the 2nd sample with reaction of MgFeSi during solidification.

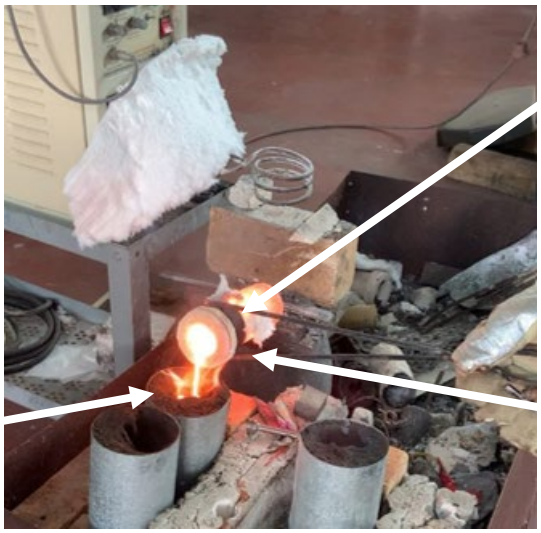

Fig. 1. Experimental setup during melting and alloying

Table 1
FeMn and FeCr (wt%), alloyed materials, nodularizer, inoculant, and chemical makeup of iron

	Element constituent										
	C	Si	Mn	P	S	Mg	Ni	Ca	Cr	R.E	Fe
MgFeSi	-	44.00	-	-	-	5.00	-	2.00	-	-	Balance
Inoculant	-	70.00	-	-	-	-	-	2.00	-	-	Balance
Pig iron	2.91	2.28	0.12	0.07	0.02	-	0.02	-	-	-	Balance
Steel	0.20	0.15	0.60	0.03	0.02	-	-	-	-	-	Balance
Nickel	-	-	-	-	-	-	99.00	-	-	-	Balance
FeMn	-	1.00	86.00	0.10	0.02	-	-	-	-	-	-
FeCr	8.00	4.00	-	0.04	0.04	-	-	-	60.0	-	-

3. Results

3.1 Microstructure evaluation

After the casting process, alloyed iron was created that had a hypoeutectic composition made up of different component alloys containing Fe, C, Si, Mn, Ni, Cr, and other elements. During solidification, a number of mechanisms took place, including the formation nucleation site, which initiated the solidification, and element solubility, which affected the segregation of the elements, to mention a few. This alloyed iron is composed of multiple phases, which were analyzed at points P1, P2, and P3 (Figure 2): austenite matrix, a mixture of iron matrix, graphite aggregate, carbides, and inclusion of impurities. Graphite solubility in austenite is limited by Ni and Si, whereas it is increased by Mn. It is thought that during solidification, the following changes

$$L \rightarrow L_1 . L_2 \rightarrow L_1 + \gamma \quad (1)$$

where γ is an austenite iron matrix, L is liquid, and L1 and L2 are liquids rich in positive and negative segregation components. The outer portion of the alloyed iron grain, such as the Last To Freeze (LTF) region, is enriched with positive segregation elements like Mn and Cr, but the core section of the grain is typically rich in Ni and Si.

Using an optical microscope to examine the samples A and B, the results showed that the graphite mixture had solidified together with the base alloy. Graphite can take the form of a mixture of nodular graphite, rosette, or flake. Additional microstructure magnification revealed a pattern resembling a two-dimensional dendritic tree. Dendrites were visible in the 2D image at the three places under examination, P1, P2, and P3 (Figure 2). Dendrites provide evidence that these branching crystals originated during the solidification process. In general, there is a notable variation in grain incidence among the three locations under analysis. The number of grains at location P1 is relatively small. This suggests that compared to the other locations, the area sampled at P1 has a lower grain density. Next, compared to P1, there is a significant increase in grain incidence in P2. This area has a higher grain density since there are more grains there. The fact that there are more grains at P2 indicates that there are either more grain nucleation sites or a more substantial grain distribution in this area.

Fig. 2. Alloyed iron of sample A and B (25 mm diameter) as allocation to examine point P1, P2 and P3

That being said, point P3 is where the most significant observation can be made. This site has a high grain occurrence, which indicates a significantly higher grain density. The fact that there are so many grains at P3 indicates that there may be a large population of grains there, possibly as a result of favorable growing and nucleation environments. The three locations of the opposing grain occurrences—P1 showing a modest number of grains, P2 showing a considerable quantity, and P3 showing a significantly bigger grain presence—indicate clear variances in the distribution and density of particles over the area under investigation.

Using ImageJ, the average grain size in samples A and B was found. The program benefited from the micrograph photo input, which in turn improved the process of calculating the grain size or area. Because the solidification stage has an impact on the solidified alloyed iron, such computations and analyses can offer important details regarding the size and distribution of the grains in the sample. The recorded average grain size results for sample A at three different points were shown in Table 2.

Table 2
Average grain size of sample A (flake graphite)

Point	Average Grain Size Sample A
P1	655.0
P2	413.3
P3	540.1

The data indicates that sample A's average grain sizes (flake shape) under various situations (P1, P2, and P3) are inconsistent. Particularly, the maximum average grain size for P1 is 665.0 µm, indicating that sample A's grains are significantly larger than those in the other conditions under this particular condition. Going on to P3, at 540.1 µm, the average grain size is more than in P2 but less than in P1. This suggests that P3 causes sample A's grains to develop moderately, resulting in middle-average grain size.

In contrast to specimen A, point P1 of specimen B has more visible graphite nodules in the material. These are distinct nodules that can have a rounded or irregular shape. The growth of graphite during sample B's solidification was determined by the presence of graphite nodules. Point P2 had the most nodular graphite in relation to the other places that were analyzed. There is a noteworthy concentration of graphite nodules at P2, which suggests that there are more of these spherical or irregular graphite structures present in this area of the material. By comparison, P3 has somewhat fewer graphite nodules than P2. While the presence of graphite nodules remains, the number has dropped marginally, indicating a little lower concentration or dispersion of these nodular graphite forms inthe material at P3 (Figure 3,4 and 5).

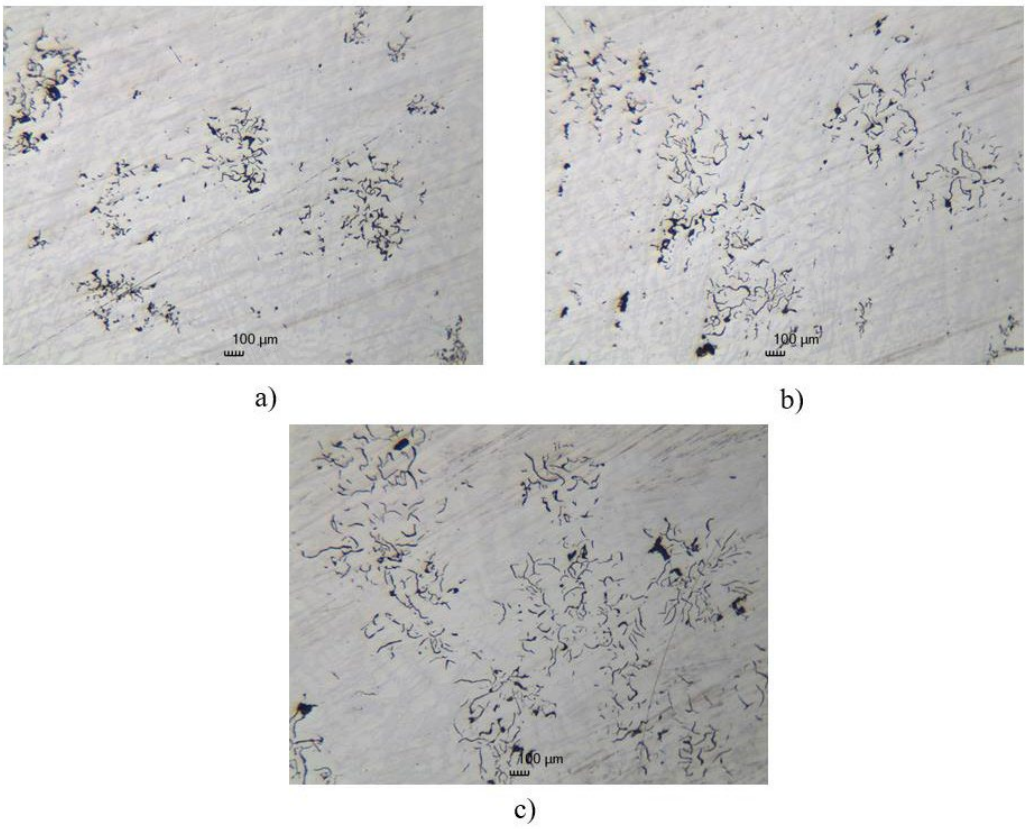

Fig. 3. Microstructure evaluation based on sample A by optical microscope on point P1, P2 and P3 revealing flake graphite shape (100x magnification)

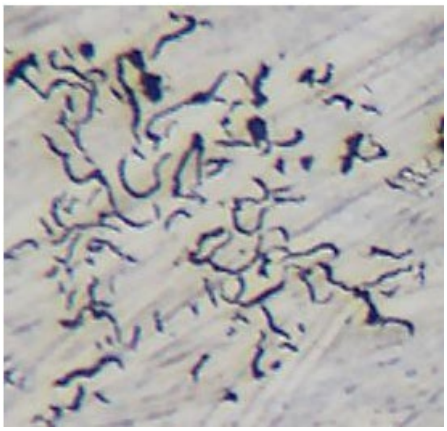

Fig. 4. Close magnification of 2D micrograph image revealing part of dendritic structure (400 magnification)

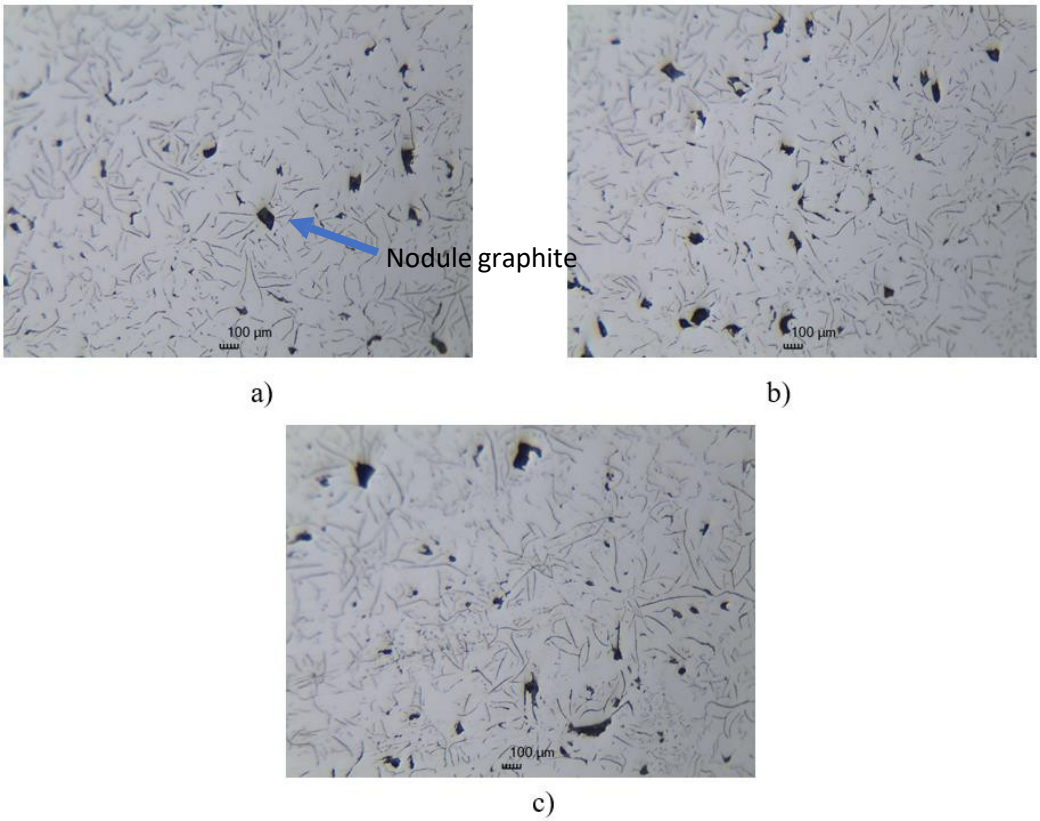

Fig. 5. Microstructure evaluation based on sample B by optical microscope on point P1, P2 and P3 revealing a mixture of flake and nodule graphite shape (200x magnification)

In addition to what has already been found, sites P3 have a higher concentration of graphite nodules than other locations. Within sample B, these graphite nodules grow into distinct structures, suggesting that graphite creation had place during the casting or solidification process. The size, shape, and distribution of these nodules can vary, adding to the overall microstructure of the material. The process of solidification, in which the carbon in the molten metal separates and crystallizes into graphite structures, is most likely what causes the graphite nodules [11].

Nonetheless, a semi-spheroidal shape has been observed in several of these graphite nodules, suggesting that they were undergoing an incomplete growth phase. This suggests that either the

formation of these graphite structures was stopped during solidification, or the graphite development process may not have been finished. The fact that the flakes in sample B are still visible suggests that the transformation into totally dendritic material has not yet taken place. The average grain size for sample B at each of the three locations is displayed in the Table 3.

Table 3
Average grain size of sample B (nodule graphite)

Point	Average Grain Size Sample B
P1	176.6
P2	266.5
P3	321.2

The graphical representations demonstrate that, among the three places, the average grain size for sample B is 176.6 µm at point P1. This suggests the presence of the smallest grain sizes. In contrast, an intermediate range of grain sizes is shown by the average grain size of 266.5 µm at point P2. At last, point P3, with an average measurement of 321.2 µm, shows the largest grain sizes.

Based on the aforementioned data, it can be inferred that sample A's flake structure has an average grain size ranging from 665.0 µm to 413.3 µm, whereas sample B's graphite structure and size average is smaller, ranging from 176.6 to 321.2 µm. Dendrites in the shape of nodules have been demonstrated to be smaller than flakes. Growth dynamics are most likely the underlying cause of nodule-shaped dendrites' smaller size than flakes [12]. The production of several branches and arms is made possible by dendritic growth, which increases the amount of surface area that may be used to accumulate more material. This branching growth method allows dendrites to continue developing in several directions, which accelerates the pace of cooling in numerous directions. Smaller average sizes are therefore anticipated [13]. Conversely, flakes typically grow more restrictedly, mostly on one plane despite their limited size. Compared to dendrites, the total sizes are larger because to the restricted development direction, which limits the available surface area for accumulation and expansion [14-16].

Using a SEM image, sample A's microstructure may be further examined (Figure 6). For sample A, there isn't a discernible dendritic structure. While image b) was taken at a magnification of 200x, providing an even closer inspection (micro view), image a) was taken at a magnification of 100x, allowing for an overall investigation of the microstructure. Upon close inspection of these pictures, it is evident that as was previously mentioned, the geometry of the flakes, not the dendrites, defines sample A's microstructure. The microstructure exhibits flake-like characteristics that suggest they originated either during the solidification process or because carbon or graphite has different properties from solidified alloyed iron.

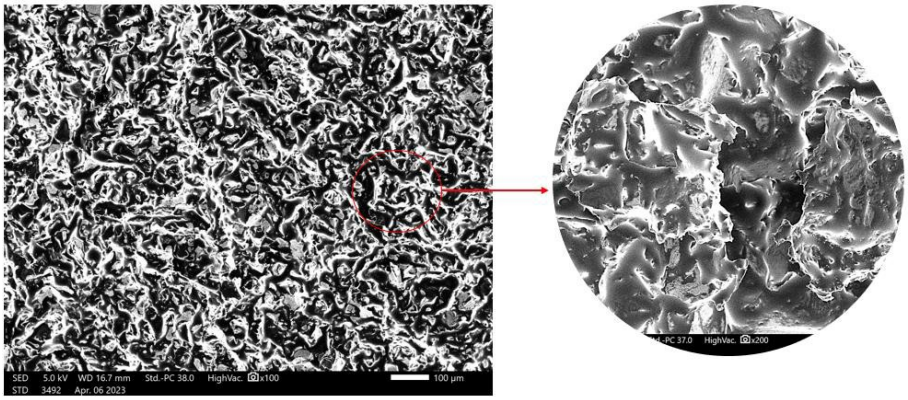

Fig. 6. Microstructure evaluation based on sample A by SEM on macro area revealing a mixture of a flake graphite shape structure

Sample B, on the other hand, exhibits a distinct dendritic structure (Figure 7). The two primary assemblies of the structure are the secondary dendritic arm spacing (SDAS) and the tree-a-like dendritic arm spacing (DAS), which is a smaller branch. The distance between a dendritic structure's separate arms or branches is referred to as dendritic arm spacing. It shows the typical distance between neighboring dendritic network arms. A number of variables, including the material's composition, production conditions, and pace of cooling, affect DAS. Dendrite arm spacing often increases with slower cooling rates and decreases with quicker cooling rates [16].

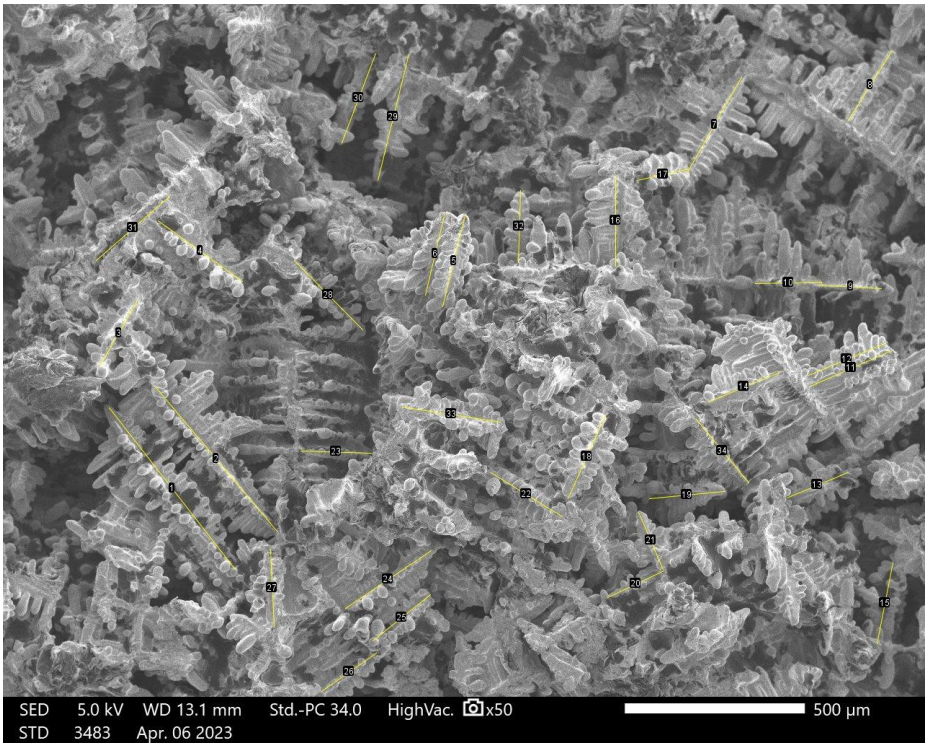

Fig. 7. Macro view of specimen B fracture surface showing unidirectional arrangement of dendriticstructure

Conversely, secondary arm spacing describes the separation between the secondary arms or branches that make up a single dendritic arm. It stands for the distance between the finer branches that split off from the main dendritic arm. The SDAS can shed light on the finer points of dendritic growth because it is usually smaller than the dendritic arm spacing (Figure 8). Due to their potential

to impact the mechanical characteristics, solidification behavior, and other material properties of the sample, dendritic arm spacing and secondary arm spacing are also significant factors in the characterization and comprehension of dendritic structures [17].

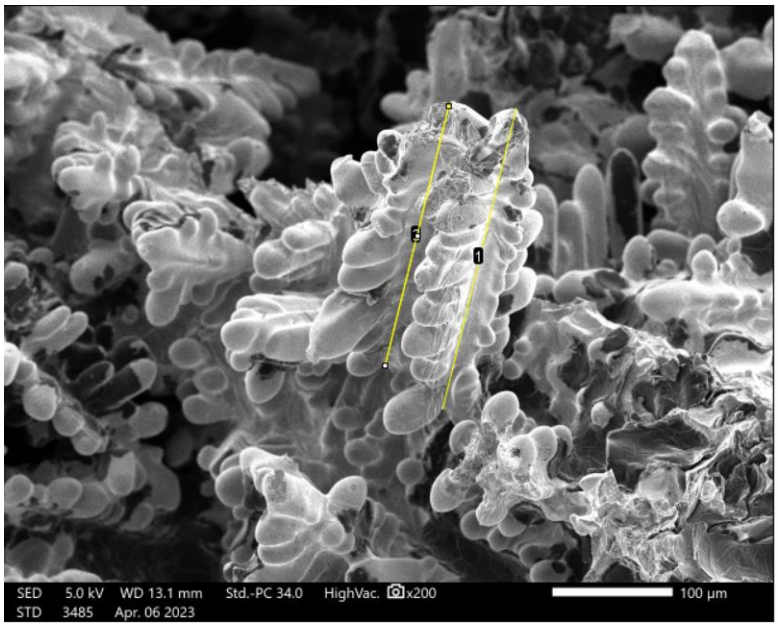

Fig. 8. Close up view of specimen B revealing dendritic structure

4. Conclusions

The treatment of magnesium during the solidification of alloyed iron in this research resulted in a nodular graphite structure rather than a flake structure (without influenced by Mg). Nodule graphite is not as round as regular ductile iron, though, because of the increased alloying element content of Ni, Cr, and Mn. A second analysis revealed that nodular graphite is not as abundant as ordinary ductile iron and that its distribution is not uniform. The influence of higher alloying elements (Ni, Cr, and Mn) during alloyed iron solidification towards graphite formation needs more research. The study also shows that iron alloyed with flake graphite lacks a discernible dendritic structure. However, at nodular graphite alloyed iron, a dendritic tree-like composition of DAS and SDAS was observed.

Acknowledgement

This research was funded by a grant from Ministry of Higher Education of Malaysia (FRGS Grant FRGS/1/2022/TK10/UMP/02/64 - RDU220135) and university's internal grant (RDU220305).

References

[1] Çelik, Gülşah Aktaş, Maria-Ioanna T. Tzini, Şeyda Polat, Ş. Hakan Atapek, and Gregory N. Haidemenopoulos. "Thermal and microstructural characterization of a novel ductile cast iron modified by aluminum addition." *International Journal of Minerals, Metallurgy and Materials* 27 (2020): 190-199. https://doi.org/10.1007/s12613-019-1876-8

[2] Xiang, Shengmei, Stefan Jonsson, Baohua Zhu, and Joakim Odqvist. "Corrosion fatigue of austenitic cast iron Ni-Resist D5S and austenitic cast steel HK30 in argon and synthetic diesel exhaust at 800° C." *International Journal of Fatigue* 132 (2020): 105396. https://doi.org/10.1016/j.ijfatigue.2019.105396

[3] Morrison, J. C. "Corrosion behaviour of Ni-Resist cast irons." *Anti-Corrosion Methods and Materials* 30, no. 8 (1983): 8-9. https://doi.org/10.1108/eb007227

[4] Fatahalla, Nabil, Aly AbuElEzz, and Moenes Semeida. "C, Si and Ni as alloying elements to vary carbon equivalent of austenitic ductile cast iron: Microstructure and mechanical properties." *Materials Science and Engineering: A* 504, no. 1-2 (2009): 81-89. https://doi.org/10.1016/j.msea.2008.10.019
[5] Jincheng, Xu. "Ecodesign for wear resistant ductile cast iron with medium manganese content." *Materials & Design* 24, no. 1 (2003): 63-68. https://doi.org/10.1016/S0261-3069(02)00076-6
[6] Choi, J. O., J. Y. Kim, C. O. Choi, J. K. Kim, and P. K. Rohatgi. "Effect of rare earth element on microstructure formation and mechanical properties of thin wall ductile iron castings." *Materials Science and Engineering: A* 383, no. 2 (2004): 323-333. https://doi.org/10.1016/j.msea.2004.04.060
[7] Jiyang, Zhou. "Colour metallography of cast iron." *China foundry* 6, no. 1 (2009): 57-69.
[8] Dias, Anderson, and Vanessa de Freitas Cunha Lins. "Scale morphologies and compositions of an iron-manganese-aluminum-silicon alloy oxidated at high temperatures." *Corrosion science* 40, no. 2-3 (1998): 271-280. https://doi.org/10.1016/S0010-938X(97)00134-0
[9] Tjong, S. C. "Electron microscope observations of phase decompositions in an austenitic Fe-8.7 Al-29.7 Mn-1.04 C alloy." *Materials Characterization* 24, no. 3 (1990): 275-292. https://doi.org/10.1016/1044-5803(90)90055-O
[10] Rashidi, Maarof Mohd, and Mohd Hasbullah Idris. "Microstructure and mechanical properties of modified ductile Ni-resist with higher manganese content." *Materials Science and Engineering: A* 574 (2013): 226-234. https://doi.org/10.1016/j.msea.2013.02.038
[11] Kim, Yoon-Jun, Ho Jang, and Yong-Jun Oh. "High-temperature low-cycle fatigue property of heat-resistant ductile-cast irons." *Metallurgical and Materials Transactions A* 40 (2009): 2087-2097. https://doi.org/10.1007/s11661-009-9911-4
[12] Stan, Iuliana, Denisa-Elena Anca, Iulian Riposan, and Stelian Stan. "Solidification pattern of 4.5% Si ductile iron in metal mould versus sand mould castings." *Journal of Thermal Analysis and Calorimetry* 148, no. 5 (2023): 1805-1817. https://doi.org/10.1007/s10973-022-11832-4
[13] Mrvar, Primož, Mitja Petrič, and Milan Terčelj. "Thermal Fatigue of Spheroidal Graphite Cast Iron." In *TMS Annual Meeting & Exhibition*, pp. 406-415. Cham: Springer Nature Switzerland, 2023. https://doi.org/10.1007/978-3-031-22524-6_37
[14] Sangame, Bahubali Babanrao, Y. Prasannatha Reddy, and Vasudev D. Shinde. "Analyzing the effect of inoculant addition on the solidification of ductile cast irons using thermal analysis." *World Journal of Engineering* ahead-of-print (2022). https://doi.org/10.1108/WJE-07-2022-0272
[15] Bauer, Branko, Ivana Mihalic Pokopec, Mitja Petrič, and Primož Mrvar. "Effect of bismuth on preventing chunky graphite in high-silicon ductile iron castings." *International Journal of Metalcasting* 14 (2020): 1052-1062. https://doi.org/10.1007/s40962-020-00419-0
[16] Liu, Jin-hai, Jian-shuai Yan, Xue-bo Zhao, Bin-guo Fu, Hai-tao Xue, Gui-xian Zhang, and Peng-hui Yang. "Precipitation and evolution of nodular graphite during solidification process of ductile iron." *China Foundry* 17 (2020): 260-271. https://doi.org/10.1007/s41230-020-0042-2
[17] Chatcharit, Kiattisaksri, Akira Sugiyama, Kohei Morishita, Taka Narumi, Kentaro Kajiwara, and Hideyuki Yasuda. "Time evolution of solidification structure in ductile cast iron with hypereutectic compositions." *International Journal of Metalcasting* 14 (2020): 794-801. https://doi.org/10.1007/s40962-020-00424-3